IL NUOVO CIMENTO **48 C** (2025) 229
DOI 10.1393/ncc/i2025-25229-4

COMMUNICATIONS: SIF Congress 2024

3D image quality of a CBCT scanner for maxillofacial intrasurgical navigation

C. COTENA(1), C. MAINARDI(2)(3), S. CLEMENTE(2), A. VARALLO(2), S. GRASSO(2), M. BUONO(2), C. OLIVIERO(2), D. MANZI(2), M. PUGLIESE(1)(3) and A. SARNO(4)

(1) *Dipartimento di Fisica "E. Pancini", Università di Napoli Federico II - Napoli, Italy*
(2) *UOSD Fisica Sanitaria e Radioprotezione AOU Federico II - Napoli, Italy*
(3) *INFN, Sezione di Napoli - Napoli, Italy*
(4) *Dipartimento di Fisica "A. Pontremoli", Università degli Studi di Milano & INFN Milano Milano, Italy*

received 28 January 2025

Summary. — This work aims to provide the first characterization of the Loop-X Cone-Beam CT scanner for maxillofacial applications, with a focus on patient dose and image quality in 3D acquisitions. Measurements were performed with adult and paediatric "head" protocols, using the dedicated Catphan604 phantom to evaluate the different parameters. Spatial resolution was assessed using the modular transfer function, with a limiting spatial frequency —evaluated at 10% of its maximum— of 0.60 mm^{-1} for the adult protocol and 0.53 mm^{-1} for the paediatric protocol (mean value). In addition, noise was characterized in terms of noise power spectrum (NPS) and contrast to noise ratio (CNR) was calculated for the adult protocol between simulated soft tissue and bone (23 ± 1) and between spinal disc and soft tissue (1 ± 1).

1. – Introduction

Intrasurgical navigation allows visualization of anatomical structures during maxillofacial surgery with the potential to reduce errors [1]. Cone-beam computed tomography (CBCT) has been shown to be a valid imaging tool in this field, due to its high effectiveness-cost ratio and flexibility [2-4]. This technology supports surgeons in following surgical instruments, such as a pointer or a surgical drill, with a high degree of precision and in real time. The CBCT scanner enables the acquisition of a 3D image of the patient and, when combined with a suitable tracking system, allows instruments to be tracked within the 3D volume during surgery. This work aims to characterize the Loop-X CBCT scanner for surgical navigation produced by Brainlab [5, 6] in terms of both 3D image quality and phantom dosimetry. Specifically, the investigations focused on acquisition protocols dedicated to 3D head imaging for maxillofacial surgical operations.

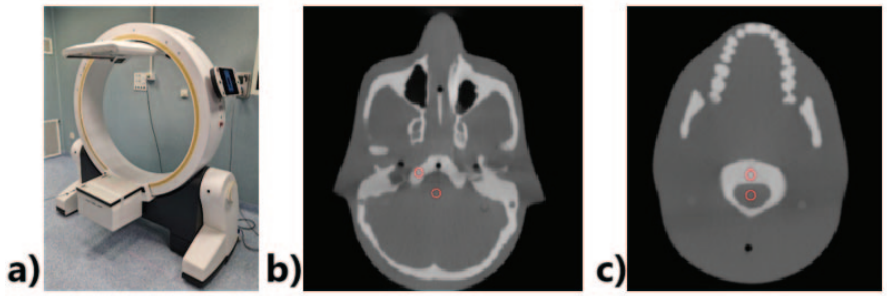

Fig. 1. – (a) Loop-X CBCT scanner. (b), (c): reconstructed axial slices of the adult ATOM phantom: (b) skull base level and (c) cervical level. ROIs identify regions for CNR evaluation.

2. – Materials and methods

The Loop-X Mobile Imaging Robot CBCT scanner is a digital X-ray system that acquires planar images, performs 3D computer tomography with cone-beam technology, and reconstructs anatomical regions of interest (fig. 1(a)). The scanner features an aluminum alloy ring gantry with a diameter of 121 cm and is equipped with two rotating arms: one for positioning the X-ray source and the other for the Varex XRD 4343 RF flat panel detector. Measurements were performed using adult and pediatric "head-skull" protocols. Both protocols operate at a voltage of 120 kV but differ in additional filtration: 0.5 mm Cu for the adult and 1.5 mm Cu for the paediatric. For both, the scan angle is 270 degrees with a reconstructed voxel size of 0.6669 × 0.6669 (mm × mm) and a slice thickness of 1.20 mm.

2˙1. *Cone-beam dose index.* – Dosimetry evaluations were performed using the cone-beam dose index (CBDI) [7]. Measurements were obtained by inserting the 10X6-3CT Radcal ionization chamber into the holes of the dedicated CTDI phantom. $CBDI_{\mathrm{w}}$ reflects the variation in the depth of the dose and was calculated according to ref. [7].

2˙2. *3D Image quality.* – Image quality was evaluated using the Catphan604 phantom. According to EFOMP and AIFM [8, 9], geometric accuracy in reconstructed slices was assessed using the four holes in the Catpahn604 phantom, which have a known distance of 50 mm. Spatial resolution was evaluated by visual evaluation of a bar pattern and by Modular Transfer Function (MTF) [8]. The highest spatial frequency clearly resolved in the bar pattern by the observer was considered the limiting resolution. The spatial resolution was also estimated from the MTF as the spatial frequency at which the curve reaches 10% of its value at 0 frequency (MTF10). The Noise Power Spectrum (NPS) was evaluated as suggested in ref. [10]. The absolute values of the 2D Fourier transform of the difference between two images of a homogeneous test object were calculated and normalized by the voxel size and ROI dimensions; the radial profile led to the 1D NPS. The Contrast to Noise Ratio (CNR) was calculated from images of the adult ATOM phantom (fig. 1(b), (c)). Circular ROIs were selected over the reconstructed slices in the tissues of interest and CNR was evaluated from the mean pixel value (μ) and standard deviation (σ) in the ROIs as follows:

$$\mathrm{CNR} = \frac{|\mu_{\mathrm{target}} - \mu_{\mathrm{background}}|}{\sqrt{\frac{\sigma^2_{\mathrm{target}} + \sigma^2_{\mathrm{background}}}{2}}}. \tag{1}$$

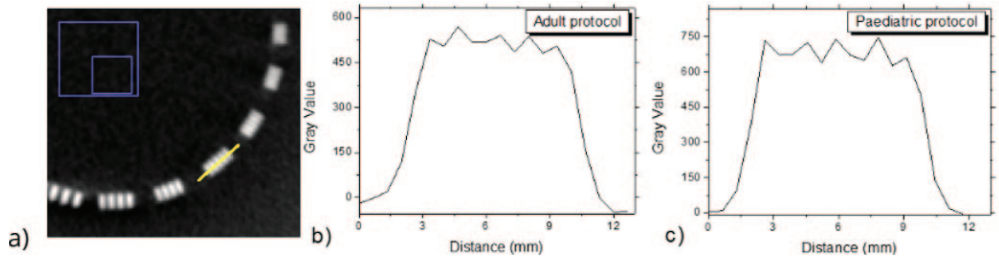

Fig. 2. – (a) Reconstructed slice containing the bar pattern within the Catphan604 test phantom. Line profile across the yellow line outlined in (a) across the 5 lp/cm bar pattern portion for the (b) adult and (c) paediatric protocols.

3. – Results

3˙1. *3D dosimetry.* – The measured values of $CBDI_{\mathrm{w}}$ for the paediatric and adult protocols resulted in $1.9 \pm 0.1\,\mathrm{mGy}/100\,\mathrm{mAs}$ and $8.0 \pm 0.3\,\mathrm{mGy}/100$ mAs, respectively. The values are consistent with those expected from the scanner in automatic exposure mode and align with the differences observed in the application.

3˙2. *3D image quality.* – In order to evaluate the geometric accuracy of the system, the distances in the x and y directions between the holes centers in the designated section of the Catphan604 test phantom were evaluated in an axial slice. According to the specifications outlined in the manual, the measured distance was estimated to be 50.00 ± 0.01 mm in both directions x and y. The spatial resolution of the system was first evaluated using the bar pattern section of the Catphan604 phantom (fig. 2), and it was determined that the system can resolve a pair of 5 lines/cm with adult and paediatric protocols.

In the second analysis, the MTF was evaluated using a tilted tungsten wire detail. The profiles of the selected ROIs were analyzed using Origin software. Figure 3 illustrates the curves obtained for five consecutive slices, showing a MTF10 ranging between 0.57 mm^{-1} and 0.65 mm^{-1} (mean value 0.60 mm^{-1}) for the adult protocol and between 0.47 mm^{-1} and 0.56 mm^{-1} (mean value 0.53 mm^{-1}) for the paediatric protocol.

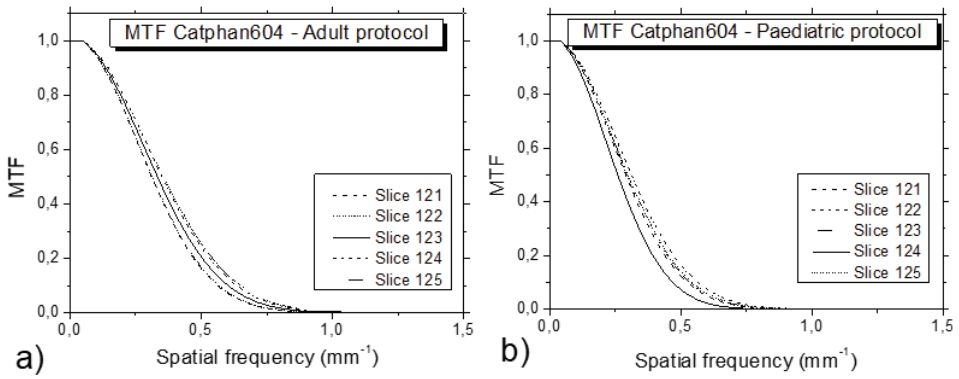

Fig. 3. – MTF curves evaluated across five consecutive axial slices for (a) the adult protocol and (b) the paediatric protocol.

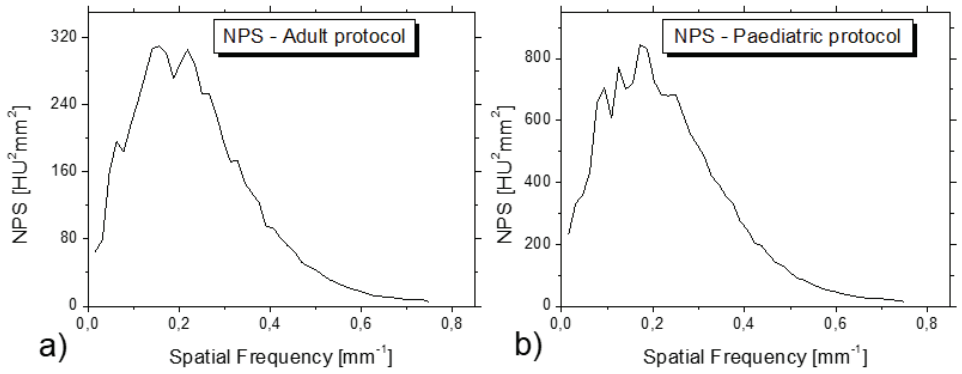

Fig. 4. – NPS curves evaluated for the (a) adult protocol and (b) paediatric protocol.

NPS curves are reported in fig. 4, for the adult and paediatric protocols. Both were evaluated for auto-exposition mode acquisition settings.

The CNR for the adult protocol between bone and soft brain tissues (fig. 1(b)) was found to be 23±1. Similarly, when calculated between the spinal disc and soft tissue it was 1±1 (fig. 1(c)).

4. – Discussion and conclusion

This paper provides the first physical characterization of the Loop-X CBCT scanner for intrasurgical navigation in maxillofacial applications. The normalized $CBDI_{\mathrm{w}}$ at 100 mAs was found to be 8.0 ± 0.3 mGy for the adult protocol and 1.9 ± 0.1 mGy for the paediatric protocol. The limiting spatial resolution in 3D images was 0.60 mm^{-1} and 0.53 mm^{-1} for the adult and paediatric protocols, respectively. Furthermore, NPS was reconstructed for both protocols, and CNR was evaluated using biological tissue-simulating phantoms. Future studies could extend this analysis to other clinical scenarios, including customized protocols and integration with advanced technologies.

* * *

The authors acknowledge the support of the Department of the MaxilloFacial Surgery of the AOU Federico II which granted access to the scanner.

REFERENCES

[1] Anand M. and Panwar S., *Clin. Cosmet. Investig. Dent.*, **13** (2021) 127.
[2] Fahrig R. *et al.*, *J. Med. Imaging*, **8** (2021) 052115.
[3] Goguet Q. *et al.*, *Oral Maxillofac. Surg.*, **23** (2019) 487.
[4] Kendlbacher P. *et al.*, *Neurosurg. Focus*, **52** (2022) E7.
[5] `https://www.brainlab.com/surgery-products/overview-platform-products/`.
[6] Karius A. *et al.*, *J. Appl. Clin. Med. Phys.*, **23** (2022) e13501.
[7] Amer A. *et al.*, *Br. J. Radiol.*, **80** (2007) 476.
[8] de las Heras Gala Hugo *et al.*, *Quality Control in CBCT, EFOMP-ESTRO-IAEA Protocol*, 2nd edition (EFOMP) May 2019.
[9] AIFM, Report AIFM No. 14 (2019).
[10] Yang K. *et al.*, *Med. Phys.*, **35** (2008) 5317.